An investigation into the tension lap splices

Yakubu M. Karkarna[1] Ali Bahadori-Jahromi[2], Hamid Zolghdr-Jahrom[3] and Emily Halliwell[4]

[1]PhD candidate, School of Computing and Engineering, University of West London, London, UK, W5 5RF
[2]Professor of Civil Engineering, School of Computing and Engineering, University of West London, London, UK, W5 5RF
[3]Senior Lecturer, University of Westminster London, London, NW1, 5LS
[4]Senior Structural Engineer, The Concrete Centre London, UK, SW1V 1HU

Abstract. The purpose of this study is to investigate the effect of lap joint length on structural performance under ultimate load using both nonlinear numerical analysis and laboratory experiments. Three-dimensional (3D) finite element models were employed for the numerical simulations, which were carried out using LUSAS software. A typical four-point bending system was modelled in order to analyze the impact of lap length. In total, 24 cases of lap length were studied across three concrete grades: C30, C45, and C60. The study also examined the influence of beam depth, shear link spacing, and concrete grade on lap joint performance. In order to validate the reliability of the 3D model, experimental data from RC beam test specimens were used.

Keywords: lap length; impact; examine; structural; lap; concrete; performance; joint; simulation

1. Introduction

The splicing of reinforcement bars is a standard practice used in concrete structures, as it is practically impossible to have continuous reinforcement bars in concrete elements due to various reasons such as steel detailing, fabrication, and transport limitations. Lap splicing, which involves the lapping of two parallel bars of sufficient length, has long been studied as an economical and effective method of splicing (ACI Committee 408, 2003).

In recent years, the required length of reinforcement laps prescribed by building codes has increased significantly from previous design recommendations, such as the now-superseded UK code BS 8110-1. This paper is motivated by the current revision of Eurocode 2, which is due to be published in 2023. The draft revision of Eurocode 2 for laps and anchorage is heavily influenced by the recommendations of the fib Model code 2010 and fib Bulletin 72.

For context, the fib Model code 2010 requires a considerably longer lap length than Eurocode 2, which many UK practitioners find excessive compared to previous UK practice. Any increase in lap length is an issue for UK designers, who already find that the current Eurocode 2 reinforcement detailing requirements are complicated and make the design costly and unsustainable (Micallef and Vollum, 2017).

The flexural capacity of reinforced concrete (RC) beams, with respect to the bond between the reinforcement and concrete, that have been lap spliced in tension under ultimate load is a matter of concern since it is crucial to the safety and strength of the RC beam (Cairns, 2016). In this regard, most design codes such as the American Concrete Institute and

Eurocode 2 specify different requirements for the design of the minimum required lap splice for a certain bar diameter. Various factors have been ascribed to lap splice failure, such as the bond between the concrete and reinforcement, concrete compressive and tensile strength, inadequate concrete cover, and lap splice length (Chu and Kwan, 2018; Lagier et al., 2015). The identified factors are based on the Eurocode 2 requirements. In recent years, the flexural capacity and behaviour of RC beams with laps located at the tension reinforcement region have been extensively investigated. Lagier et al. (2015) studied the bond strength of an ultra-high-performance fibre RC specimen lap spliced in tension using the Canadian design code. Their results suggest that splitting failure in concrete beams due to reinforcement laps could be attributed to inadequate tensile properties of the concrete cover, which is a function of the overall strength of the concrete.

Diab (2008) experimented on 12 normal strength concrete beam specimens, considering variables such as type, spacing, shape of spacing, and shape of transverse reinforcement in the lapped region embedded in normal strength concrete, among others. He concluded that there was a drastic increase in the ductility of beams when transverse reinforcement was used. Mousa (2015) studied the flexural behaviour and ductility of high strength concrete beams with tension lap splice using the American code (ACI) and found that the bond strength of the lapped reinforcement bars was mainly dependent on the steel yield strength, diameter of reinforcement, concrete cover, shape of reinforcement lap ends, surface of the reinforcement bar, and reinforcement lap length. Deng, Ma, et al. (2021) and Deng, Li et al. (2021) studied the flexural and shear behaviours of RC reinforced beams strengthened by the prestress carbon fibre-reinforced polymer prestressed concrete prisms. The experimental

Yakubu M. Karkarna, Ali Bahadori-Jahromi, Hamid Zolghadr Jahromi
*and Emily Halliwell*
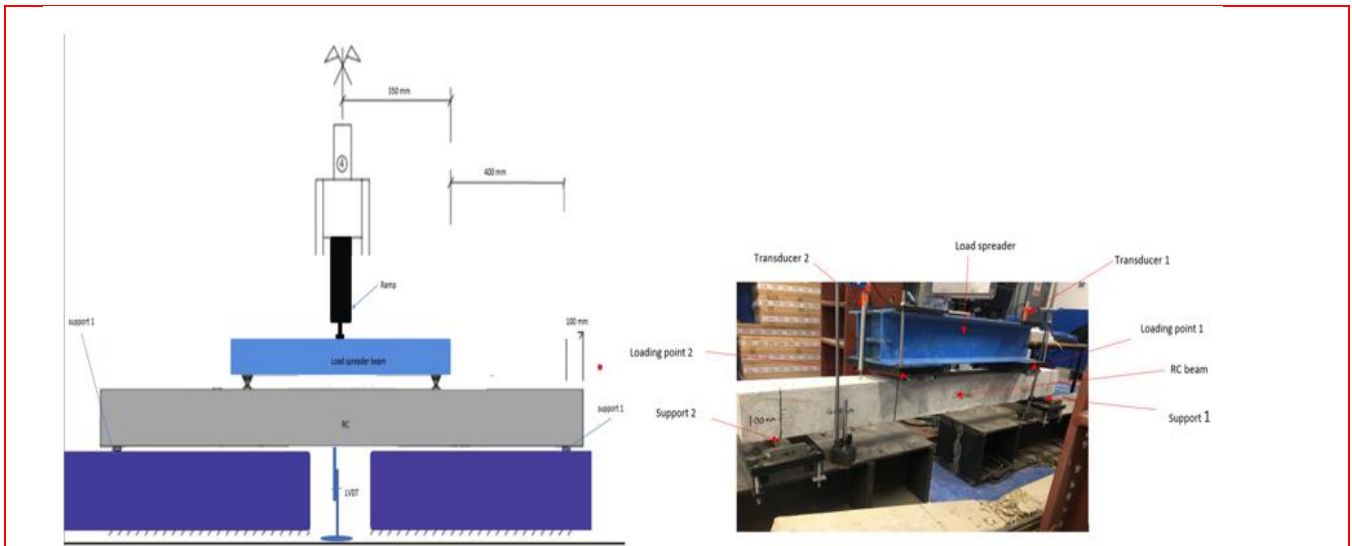
Fig. 1 Typical laboratory four-point loading arrangement

studies have revealed that the bond strength plays an important role in the ultimate strength of the beams. Ahmed (2013) studied the effect of the splice length, concrete compressive strength, and the amount of transverse reinforcement within the lap splice zone. The outcomes indicated that providing shear links within the lap splice region increased the beam's ductility and ultimate load capacity.

This study aims to investigate the impact of varying lap joint length on the structural performance of RC beams under ultimate load by using LUSAS finite element software to simulate a four-point loading test under monotonic loading until failure (see Figure 2). The variables utilised in this computational study conform to Eurocode 2, including the reinforcement bar diameter (db), concrete design tensile strength ($fctd$), concrete cover (cd), and yield strength of the steel (fy).

2. Methodology

The study analysed five series of reinforced concrete beams (A, B, C, D, and E) with lap splices located in the maximum moment zone, as shown in Figure 1 and detailed in Table 1. The beams with varying lap lengths had dimensions of 1700 mm in length, 150 mm in height, and 150 mm in width, with a span-to-depth ratio of 11.3 for all series except E and F, which had a zero-shear span distance of 500 mm and 300 mm, respectively, with the same span-to-depth ratio.

As shown in Figures 2(a), (b), and (c), each sample's tension face was reinforced with three bars, 12 mm in diameter, lapped with bars of the same diameter. All laps were located in the same section, as permitted by MC2010 and BS EN 1992-1-1:2004, but they were not staggered as recommended by Eurocode 2. For all series except D, nominal 8 mm diameter shear links were provided at 100 mm spacing, while for series D, 50 mm link spacing was used. The transverse reinforcement met the requirements of Eurocode for all series.

Three different concrete grades (C30, C45, and C60) were used for all series, and the two-point loads were fixed at a distance of 700 mm for all series except E, where the distance was decreased to 500 mm to accommodate the lap splices within the loading points.

Series	Test ID	Bar diameter (mm)	Lap length (mm)	Concrete grade	Link spacing (mm)	Depth (mm)	Distance between point loads (mm)	Span/depth ratio
A	4P-Control	12	n/a	C30	100	150	700	11.3
	4P- 30Ø	12	360	C30	100	150	700	11.3
	4P- 40Ø	12	480	C30	100	150	700	11.3
	4P- 50Ø	12	600	C30	100	150	700	11.3
	4P-EC2 (62Ø)	12	744	C30	100	150	700	11.3
B	4P- 30Ø	12	360	C45	100	150	700	11.3
	4P- 40Ø	12	480	C45	100	150	700	11.3
	4P- 50Ø	12	600	C45	100	150	700	11.3
	4P-EC2 (62Ø)	12	744	C45	100	150	700	11.3
C	4P- 30Ø	12	360	C60	100	150	700	11.3
	4P- 40Ø	12	480	C60	100	150	700	11.3
	4P- 50Ø	12	600	C60	100	150	700	11.3
D	4P- 30Ø	12	360	C30	50	150	700	11.3
	4P- 40Ø	12	480	C30	50	150	700	11.3
	4P- 50Ø	12	600	C30	50	150	700	11.3
	4P-EC2 (62Ø)	12	744	C30	50	150	700	11.3
E	4P- 30Ø	12	600	C30	100	150	500	11.3
	4P-40Ø	12	480	C30	100	150	500	11.3
	4P-50Ø	12	600	C30	100	150	500	11.3
	4P-EC2 (62Ø)	12	600	C30	100	150	500	11.3
F	4P- 30Ø	12	300	C30	100	150	900	11.3
	4P- 40Ø	12	480	C30	100	150	900	11.3
	4P- 50Ø	12	600	C30	100	150	900	11.3
	4P-EC2 (62Ø)	12	744	C30	100	150	900	11.3

3. Experimental Program

The experimental beam specimens in this study were simply supported and subjected to four-point loading. The beam had a shear span of 700 mm and a span of 1500 mm between supports, as shown in Figure 2. The beams were loaded incrementally until failure was reached. They were designed in accordance with Eurocode 2 and had a compression reinforcement consisting of two φ 8 mm bars and a tension reinforcement of three φ 12 mm bars. The beams were also equipped with shear links spaced at 100 mm intervals, consisting of 8 mm diameter bars.

3.1 Materials

All specimens were tested with concrete mixed in the University of West London concrete laboratory, using the same mix design for all samples (see Figure 4). The concrete had a target mean compressive strength of 30 N/mm² and was composed of coarse aggregate (10 mm gravel), fine aggregate (sharp sand), and cement (blue circle general purpose) in the following proportions: aggregate/cement ratio of 4.2, coarse/fine sand ratio of 1, and water/cement ratio of 0.45 (as shown in Fig. 4 and Table 2).

Fig. 4 Details of concrete materials

Yakubu M. Karkarna, Ali Bahadori-Jahromi, Hamid Zolghadr Jahromi
and Emily Halliwell

Table 2 Concrete Mixture									
W/c	Total Aggregates (kg)	Water % of Mix	Water quantity (L)	Cement % of Mix	Cement quantity (Kg)	Coarse % of Mix	Coarse quantity (Kg)	Cement % of Mix	Cement quantity (Kg)
0.45	106.9	7.85	8.40	19.64	21.0	49.11	52.50	27.23	23.39
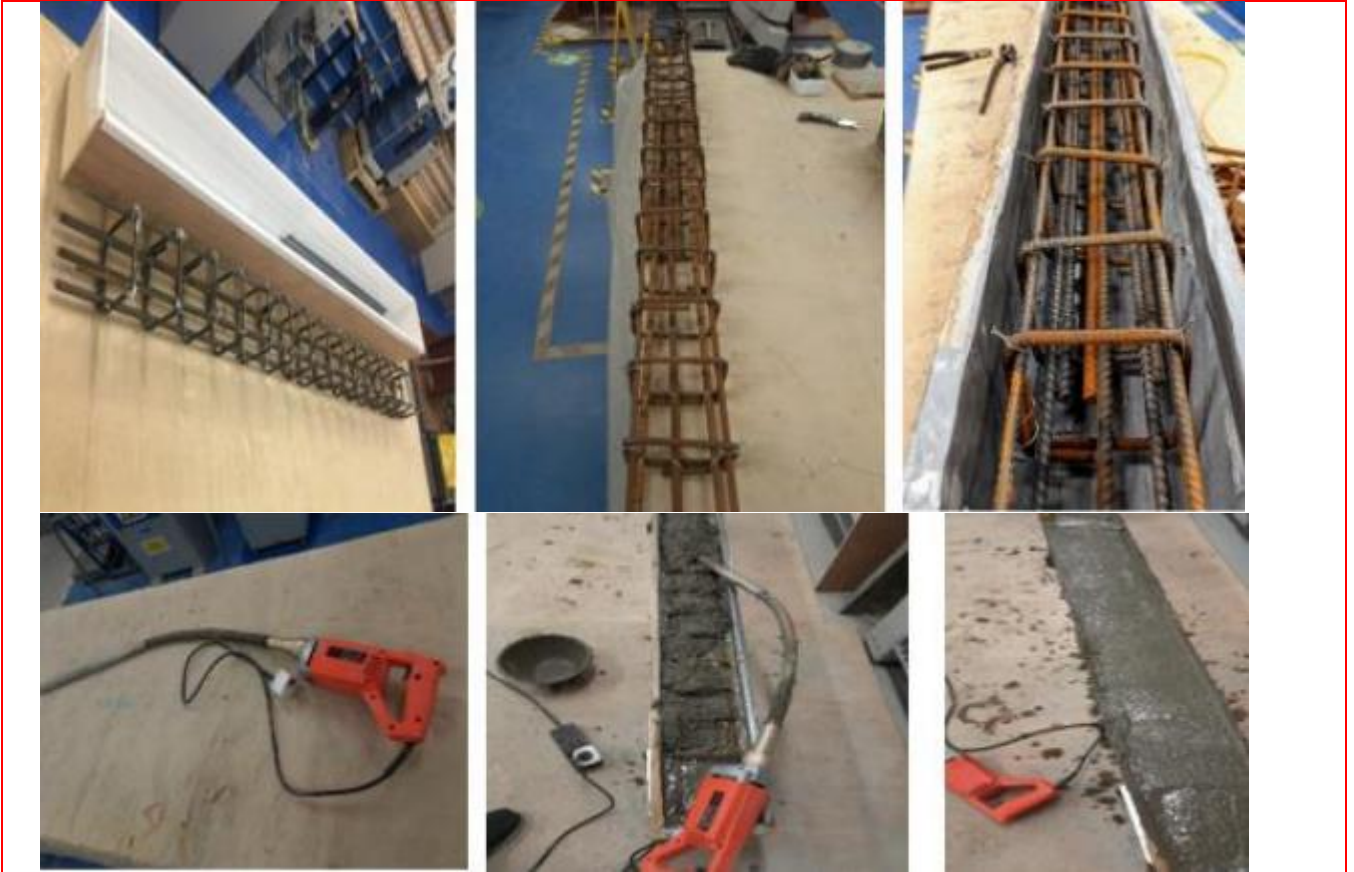
Fig. 5 Sample casting

3.2 Details of the reinforcing bars

The mild reinforcing bars utilised in the test program were rib bars with diameters of 8 mm and 12 mm, conforming to BS EN 1992-1-1:2004, which were sourced from a reputable local supplier (Metal4U). The reinforcing steel bars were supplied in 6 m lengths and were cut into various lengths in the laboratory, with careful consideration given to excluding any damaged bars from the lapped section of the beam specimens. The steel bars were used in their as-delivered state without any surface preparation or special cleaning. The link cages were fabricated using 8 mm diameter reinforcing bars sourced from the laboratory's stocks.

3.3 Casting procedure

All the beams were cast using the same mix design. The concrete mix was prepared using an ELE Concrete Mixer 34-3540, and it was mixed for 5 minutes to ensure proper homogeneity. After the concrete mix was completed, a slump test was conducted according to British Standard using the 'ELE international Slump testing kit' to assess the workability of the concrete.

Once the slump test was completed, the beams were cast separately using marine plywood as the formwork. The tension rebars were horizontally placed in the beams. The reinforcement cage was positioned within the mould and held in place during casting by a 15 mm concrete cover connected to the sides and bottom of the cage. In the lap test specimens, the lapped longitudinal reinforcement was positioned at the bottom of the formwork.

The concrete was cast in two layers, with each layer being compacted using a mechanical vibrator poker to ensure proper consolidation. The top surface of the beams was then smoothed off using a stainless-steel float to achieve a smooth finish, as shown in Figure 5.

Three-cylinder samples (150 × 300 mm) and three small beam samples (150 × 150 × 750 mm) were cast simultaneously with the main beams using the same fresh concrete. The cylinder samples were used for compressive strength testing to determine the compressive strength of the concrete, while the small beam samples were used for tensile strength testing.

Compressive strength testing was conducted on the cylinder samples in accordance with standard procedures to

assess the concrete's ability to withstand compression. Tensile strength testing, on the other hand, was performed on the small beam samples to evaluate the concrete's capacity to resist tension.

By casting and testing these additional samples in parallel with the main beams, a comprehensive assessment of the concrete's performance characteristics, including both compressive and tensile strengths, was obtained to ensure reliable and accurate results for the overall experimental program.

4 Finite Element Model

The beam model was designed to simulate a four-point bending test configuration, where the loads were applied through a two-point load in displacement control, as illustrated in Figure 3. Finite element software (LUSAS version 2018) was utilized to model the analyzed beams in 3-D. In order to focus on the maximum moment region of the beams, where the reinforcing bars are lapped, the symmetric requirement of the constraint and load was not utilized in the modeling process. This approach was chosen as it aligns with the main focus of the current study. Implementing a symmetric boundary condition to the modeled half of the beam would deviate from the scope of this study, and therefore was not employed in the analysis.

4.1 Geometric Nonlinearity

The implicit of small displacements in linear elastic analysis may not be valid in many problems, and to obtain accurate results, the impact of geometric variation of the structure during deformation, also known as geometric nonlinearity, must be considered. In LUSAS software, there are five methods available for accounting for geometric nonlinearities: Updated and Total Lagrangian, Eulerian, co-rotational, and P-Delta.

The Updated Lagrangian formulation continuously updates the structure's geometry with reference to the end of the last converged increment. The Total Lagrangian formulation relates the displacement of the structure to the initial geometric configuration throughout the solution. The Eulerian formulation has its reference in the current configuration, while the co-rotational formulation relates large displacement effects to the set axes that follow and rotate with the elements. The P-Delta method takes into account the interaction between the vertical and horizontal sway loading.

In this research, the Total Lagrangian technique has been employed. This approach has the advantage of formulating the element shape functions only once at the beginning of the analysis, which makes the method more computationally efficient compared to other methods that may require repetitive computations during the analysis.

4.2 Element Type

In the model, the concrete elements were represented using 3D isoperimetric solid continuum elements with 20-noded elements, allowing for three degrees of freedom (U and V displacements in both directions) at each node. Full numerical integration, specifically 3 × 3 Gaussian for quadrilateral elements, was utilized for accurate calculations.

On the other hand, the reinforcement was modelled using a quadratic 3D bar element (BRS3) with three nodes. This element only accounts for longitudinal forces, lacks bending stiffness, and transfers only axial stress. The displacement U and V at each node are considered as variables, and the cross-sectional area is consistent with the area of the reinforcement steel. The interface between the concrete and reinforcing bar assumes a perfect bond, and the nodal degrees of freedom are superimposed at this interface.

Figure 6(a) and (b) display the finite element used in the model, representing the BRS3 and HX20 elements.
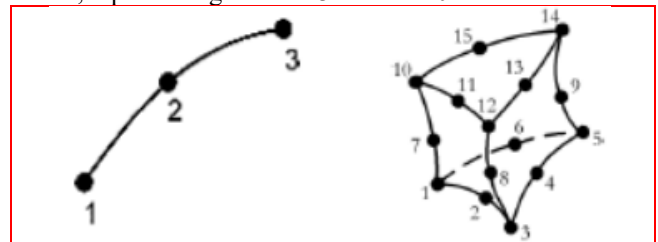
Fig. 6 Details of bar element BRS3 and plane stress element HX20 (LUSAS, 2016)

The embedded modelling approach was employed in this study to simulate the steel bars. Both the reinforcement and concrete were represented using the same type of elements, with identical degrees of freedom and shape functions, as well as an equal number of nodes. Consequently, the embedded method involved integrating a one-dimensional bar into either two-dimensional or three-dimensional elements, as depicted in Figure 7.
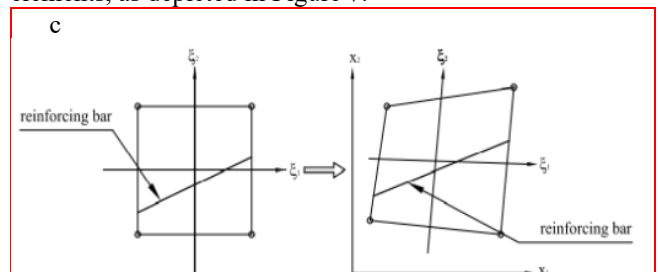
Fig. 7 Embedded reinforcing bar element in the local and global system

The computation of embedded reinforcing bars is carried out by integrating along the curves that represent the segments of the reinforcing bars within each element. Subsequently, the embedded reinforcing bar elements are superimposed onto the concrete elements in question. Unlike traditional methods, the embedded reinforcement representation does not require the reinforcement bars to match the boundary of the concrete elements. Instead, the reinforcement bars pass through the concrete elements in an arbitrary manner, allowing for flexibility in the reinforcement layout during finite element mesh generation.

One significant advantage of the embedded representation is that it enables the simulation of perfect bond between the steel and concrete, as both the concrete and reinforcing bar elements are assigned the same degrees of freedom. Thus, bond slip can only be implicitly simulated by modifying the steel or concrete constitutive relations.

Yakubu M. Karkarna, Ali Bahadori-Jahromi, Hamid Zolghadr Jahromi
and Emily Halliwell

However, it is important to note that this method requires the use of specific reinforcing bar elements.

It should be emphasised that the embedded representation is the only suitable approach for accurately simulating lap joints or lap/splice length using LUSAS, in order to address the objectives of this research.

4.4 Concrete Material

Several concrete material models are available in LUSAS for simulating the behavior of structural concrete. Two commonly used models are Model 86, which is a linear model with creep and shrinkage, and Model 109, which is a smoothed multi-crack model. Model 86 is based on a simplified linear approach with creep and assumes that the service stress in the concrete is not exceeded. On the other hand, Model 109 considers nonlinear behavior in compression and tension, including cracking and crushing.

Model 109, based on continuum damage mechanics, allows for the simulation of the nonlinear stress-strain behaviour of concrete up to failure. It considers two failure modes: crushing in compression and cracking in tension. The material behaviour is described in terms of elastic, plastic, tensile, and compressive properties. In tension, the strain-stress behaviour for concrete is simulated as a nonlinear relationship up to the ultimate tensile strength, followed by a gradually unloading branch that accounts for tension stiffening effects (Figure 9). Tension stiffening refers to the phenomenon in which concrete continues to withstand certain tensile loads despite the formation of cracks, with a slow decrease in tensile strength with an increase in tensile strain. The unloading branch of the stress-strain model in LUSAS can be represented using a nonlinear, linear, or bilinear relationship.

In this study, the stress-strain relationship proposed by LUSAS (2016) is used for the unloading failure branch, as described in equation (1) and illustrated in Figure 8. This nonlinear equation incorporates control parameters such as the associated strain (ε_{ti}), stress at first damage (f_{ti}), strain at the effective end of the curve (ε_0), uniaxial strain (f_t), and strain at peak stress (ε_k), as shown in Figure 8 in terms of fracture stress (f_s) and the strain parameter (ψ). This function has been widely used by many researchers in previous studies, providing reliable predictions of experimental response (e.g., Bencardino and Condello, 2014; Yuan et al., 2016; Guizani et al., 2017; Fib Model Code Concr. Struct. 2010, 2013; do Carmo & Lopes, 2005; LUSAS, 2015).

4.5 Solution Approach

The solution of the nonlinear equations in LUSAS is achieved using a Newton-Raphson based iterative technique. LUSAS offers two approaches for this purpose: (1) modified Newton-Raphson and (2) full Newton-Raphson. The main difference between the two techniques is that modified Newton-Raphson reuses a previous stiffness matrix, whereas the stiffness matrix is updated after each iteration in the full Newton-Raphson technique. This leads to faster convergence in the full Newton-Raphson method as the stiffness matrix is more accurately updated at each iteration. On the other hand, the modified technique may require more equilibrium iterations and thus have a slower convergence rate due to less

accurate stiffness prediction. However, with a realistic initial estimation and the use of acceleration methods such as line searches, the modified technique can also be quite rapid.

The incremental-iterative solution in LUSAS is based on the Newton-Raphson iteration, as used in this paper, where the load is slowly increased in increments to achieve equilibrium at each increment. LUSAS provides three incremental procedures: displacement-controlled, arch-length controlled, and load methods. It is also possible to combine the load and displacement methods with the arch-length method, allowing for changes in the iteration method at a given point. The incremental solution procedure can be specified in three ways: automatic, through predefined load curves, and manual. In this research, the automatic procedure was used for actual analyses, where LUSAS automatically reduces the step length by a predefined factor if convergence is not achieved within the increment after a specified number of iterations. This means that the increment size is automatically adjusted by LUSAS based on the convergence history, with a maximum number of iterations permitted before automatic step reduction set to 10. It should be noted that LUSAS allows the user to control the incrementation by specifying the starting increment size and the maximum change in increment size.

There are several convergence criteria used in the program to monitor convergence, and the adoption of suitable convergence criteria is crucial. In this research, the following criteria were used as reference: Euclidean incremental displacement norm (dtnrm = 1.0), Root mean square of residuals (RMS = 108), Work norm (wdnrm = 108), Maximum absolute residual (MAR = 108), Euclidean displacement norm (dpnorm = 1.0), and Euclidean residual norm (rdnrm = 0.1). If the tolerance limit is imposed, convergence of the generic load increment is considered satisfactory based on these parameters.

$$f_s = f_{ti} \cdot fuc(\varsigma) = (1 - \omega(\varsigma))E\varsigma \tag{1}$$

With
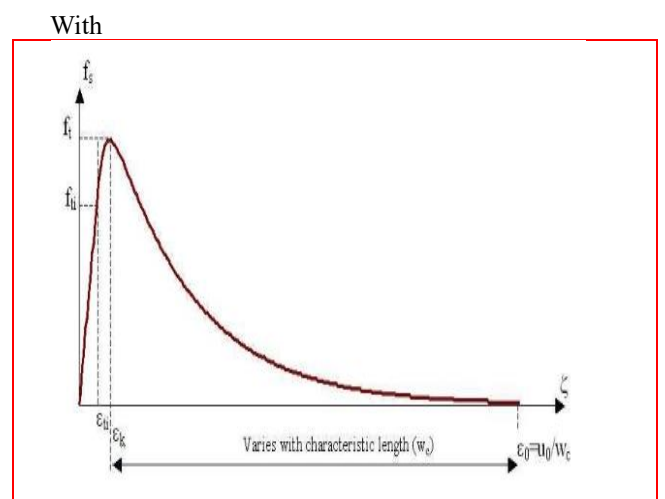
Fig. 8 Damage evaluation function (softening curve) LUSAS, 2016)

$$\omega = 1 - \frac{\varepsilon_{ti}}{\varsigma} e^{-c_1\eta}(a - be^{-c_1 m\eta} - ce^{-c_1 mp\eta}) \tag{2}$$

The form used to derive the contact is the direct relationship between f_s and ς:

$$f_s = f_{ti}e^{-c_1\eta}(a - be^{-c_1m\eta} - ce^{-c_1mp\eta}) \quad (3)$$

In which $\eta = \frac{\varsigma - \varepsilon_{ti}}{\varepsilon_0 - \varepsilon_{ti}}$

C and p are both assumed to be fixed at 5. The constants a, b, c, and m are determined from the following four conditions.

$$f_s = f_{ti} \qquad \text{at } \eta = 0 \quad (4)$$

$$\frac{\partial f_s}{\partial \varsigma} = E \qquad \text{at } \eta = 0 \quad (5)$$

$$f_s = f_t \qquad \text{at } \eta = \eta_k \quad (6)$$

$$\frac{\partial f_s}{\partial \varsigma} = 0 \qquad \text{at } \eta = \eta_k \quad (7)$$

The mean uniaxial tensile strength (f_{ctm}) can be calculated as follows (BS EN 1992-1-1, 2004):

$$f_{ctm} = 0.3(f_{ck})^{\frac{2}{3}} \text{ Where } f_{ck} = \text{ is the cylinder characteristics strength} \quad (8)$$

To estimate the (f_{ctm}) from the mean flexural strength $f_{ctm,fl}$, the following expression is adopted:

$$f_{ctm} = \alpha_{fl} \times f_{ctm,fl} \quad (9)$$

Where:

$$\alpha_{fl} = \frac{0.06 \times h_b^{0.7}}{1 + 0.06 \times h_b^{0.7}} \quad (10)$$

h_b is the beam depth (mm).

For the compression behaviour, Model 109 requires the peak compressive stress (ε_c) to be estimated as follows:

$$\varepsilon_c = 0.002 + 0.001\frac{(f_{cu}-15)}{45}$$
$$0.002 \leq \varepsilon_c = 0.003$$
$$\text{Where } f_{cu} = 1.25f_c \quad (11)$$

ε_c = Strain at peak uniaxial compression

f_c = Uniaxial compression strength
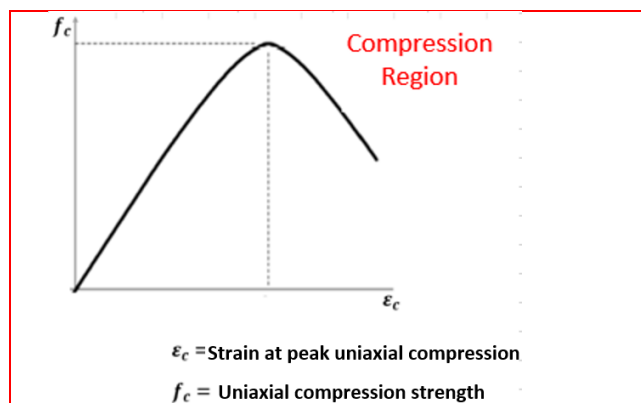
Fig. 9 Post-failure stress-strain relationship (LUSAS, 2016)

Similarly, for the compression behaviour, the model given in Eurocode 2 (BS EN 1992-1-1, 2004) and the Fib Model Code for Concrete Structures (2010) are adopted, given by following expressions:

$$\sigma_C = \left(\frac{\kappa\eta-\eta^2}{1+(\kappa-2)\eta}\right)f_{cm} \quad \text{this equation is valid for} \quad (12)$$
$$0 < |\varepsilon_c| < |\varepsilon_{cu1}|$$

Where:

ε_{cu1} is the nominal ultimate strain.

ε_{c1} is the strain at peak stress.

ε_c is the compressive strain in the concrete.

f_{cm} is the ultimate compressive strength of the concrete, given as:

$$f_{cm} = f_{ck} + 8 \ (MPa) \quad (13)$$

While the parameters η and k are calculated from equations (14) and (9), respectively:

$$K = 1.05E_{cm}\frac{|\varepsilon_{c1}|}{f_{cm}} \quad (14)$$

$$\eta = \frac{\varepsilon_c}{\varepsilon_{c1}} \quad (\varepsilon_c < 0) \quad (15)$$

In which E_{cm} is the elastic modulus of the concrete and ε_{c1} is the strain at the peak stress and E_{cm} calculated from equations (16) and (17), respectively:

$$E_{cm} = 22\left[\frac{f_{cm}}{10}\right]^{0.3} \text{s} \quad (16)$$

$$\varepsilon_{c1}(^0/_{00}) = 0.7(f_{cm})^{0.31} \leq 2.8 \quad (17)$$

The normal ultimate strain (ε_{cu1}) expressed as a percentage:

$$\varepsilon_{c1}(^0/_{00}) = 2.8 + 27\left[\frac{(98 - f_{cm})}{100}\right]^4 \quad (18)$$

Model 109 requires assigning the compressive damage

parameter at each inelastic strain increment, starting from 0 for uncracked material and progressing to 1 when the concrete completely loses its load-bearing capacity. As illustrated in Figure 60, this parameter is determined by analyzing the stress-strain diagram of concrete in compression, as shown below.

The effective end of the softening curve parameter (ε_o), if set, is calculated as:

$$\varepsilon_c = 0 \quad \text{for} \quad \varepsilon_o \approx 5G_f / W_c f_t \tag{19}$$

Where W_c is a characteristic length for the element.

The fracture energy (G_f) can be determined using the following equation:

$$G_f = k_b^2 \times c_f \times f_{ct} \tag{20}$$

In which k_b accounts for the reinforcement size related to the beam size, while the parameter c_f considers all the secondary effects. The parameter k_b is determined using the following relationship:

$$k_b = \sqrt{\frac{k.\left(2 - \frac{b}{B}\right)}{1 + \frac{b}{B_{10}}}} \tag{21}$$

The nonlinear behaviour in compression is governed by the following parameters: uniaxial tensile strength, biaxial to uniaxial stress ratio (1.15), strain at peak uniaxial compression (2.2E-3), dilatancy factor (ψ=-0.1), initial relative position of yield surface (0.6), contact multiplier on $\varepsilon0$ for first opening stage (0.5), constant in interlock state function (0.3), angular limit between crack planes (1.0 rad), and final contact multiplier on $\varepsilon0$ (5.0). Further parameters are the slope of friction asymptote for damage (μ=0.8) that define the surface of local damage and the shear intercept to tensile strength (rσ=1.25). These values were adopted based on the LUSAS manual recommendations. For the plastic phase, the capacity of the cracked concrete to transmit tensile stresses (strain softening) is considered as well as the ability to transfer shear. The softening behaviour follows an exponential descending law based on two parameters: the slope at the end of the softening curve (3.5E-3) and the uniaxial tensile strength of concrete (2.8 MPa), whose value is linked to the behaviour of the ductile element. The input parameters for the elastic phase are the Poisson ratio (0.2) and the young's modulus (31000 MPa), calculated based on Eurocode 2 (2004).

4.6 Convergence criteria

Realistic convergence criteria must be used to end the iterative procedure in order for any iteratively based solution method to be effective. If the tolerances are too tight, computational effort will be wasted obtaining needless accuracy, and- if the criteria are too loose, inaccurate results will be obtained. Given that the method computes incremental displacements by removing out of balance forces after each iteration, it seems reasonable to require that these factors be verified for convergence to zero. The Euclidean

residual norm as percentage of the total reactions such that

$$Y_g = \frac{(\Sigma\Delta g_1^2)^{1/2}}{(\Sigma\Delta R_{1+1}^2)^{1/2}} \times 100 \tag{22}$$

And the Euclidean displacement norm as percentage of the total displacement are the two parameters utilised to control convergence in the current study

$$Y_\delta = \frac{(\Sigma\Delta\delta_1^2)^{1/2}}{(\Sigma\Delta\delta_{1+1}^2)^{1/2}} \times 100 \tag{23}$$

To determine when the required accuracy is achieved, these values are compared to the input parameters. It is a good idea to verify the results after each increment for divergence to avoid wasting computer time searching for an unachievable solution. This check, like the convergence criterion, should be realistic to avoid the problem being terminated prematurely. When a certain number of iterations has been reached in LUSAS, the residual norm and Euclidean displacement percentages are checked. The problem is continued if the values are not excessively large (that is more than 100), because convergence can be reached in subsequent increments.

5.0 Result and Discussions

This The load-deflection curves (Figure 10) can be used to describe the global response of the tested beams; note that the load includes the effect of the steel beam (0.98KN) placed on the specimen and the equivalent bending moment owing to the self-weight of the tested reinforced concrete beam. During the transition from the uncracked to the cracked stage, a gradual non-linear behavior could be seen. Within the constant moment zone, several vertical cracks developed first followed by shear cracks near to the support. Figure 10 shows the comparison of the numerical and experimental results, in terms of loadmidspan deflection curves of the beams. The outcome of the experimental investigation shows that the control beam failed at the ultimate load of 65.1 KN, in a flexural mode with yielding of tension reinforcement, followed by crushing of concrete in the compression zone. For the finite element model, the control beam analysis was stopped because the limit displacement of the control point was reached. The experimental outcomes are reproduced in a satisfactory manner by the proposed finite element model with an acceptable tolerance for the current work (3% for the ultimate load values). Usually, the numerical values of the loads at the critical stages are slightly lower than the same loads detected experimentally. This proves that the 3D-model is reliable.

| (a)   Eurocode 2(FE) vs EC2 experiment | (b) Load curves of all experimental samples |
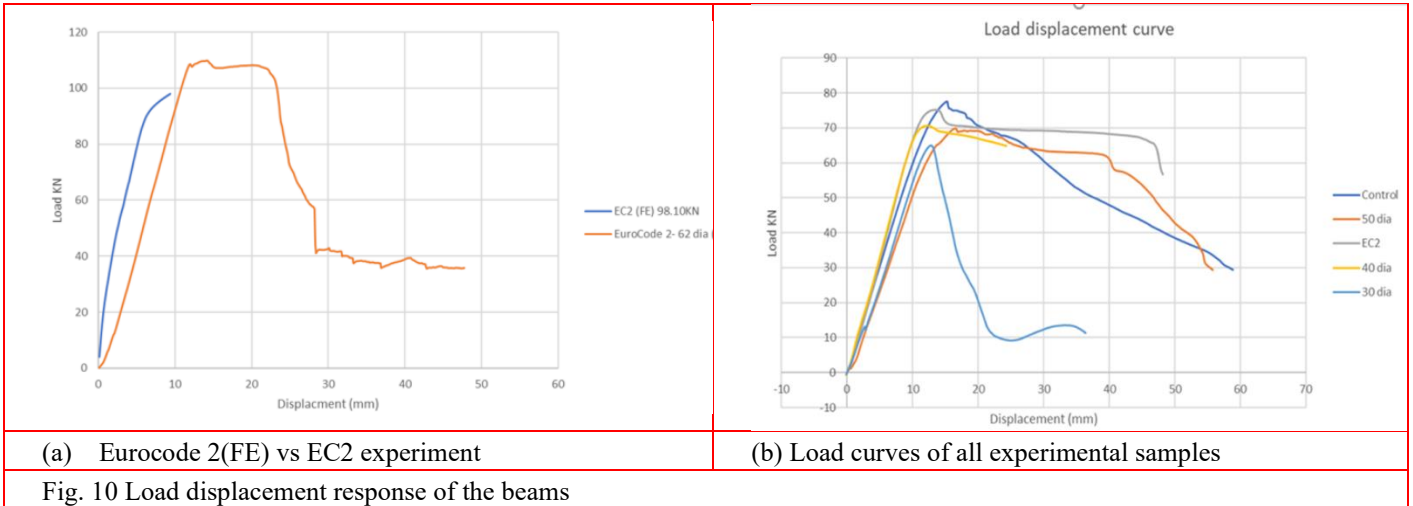
Fig. 10 Load displacement response of the beams

5.1 Parametric analysis

experimental studies (Anwar Hossain, 2008; Kim et al., 2019; Kim et al., 2013; Yang et al., 2012). This can be attributed to the fact that the bar stress is uniformly

| (a)   Lapped to bar diameter ratio | (b) Concrete grade |
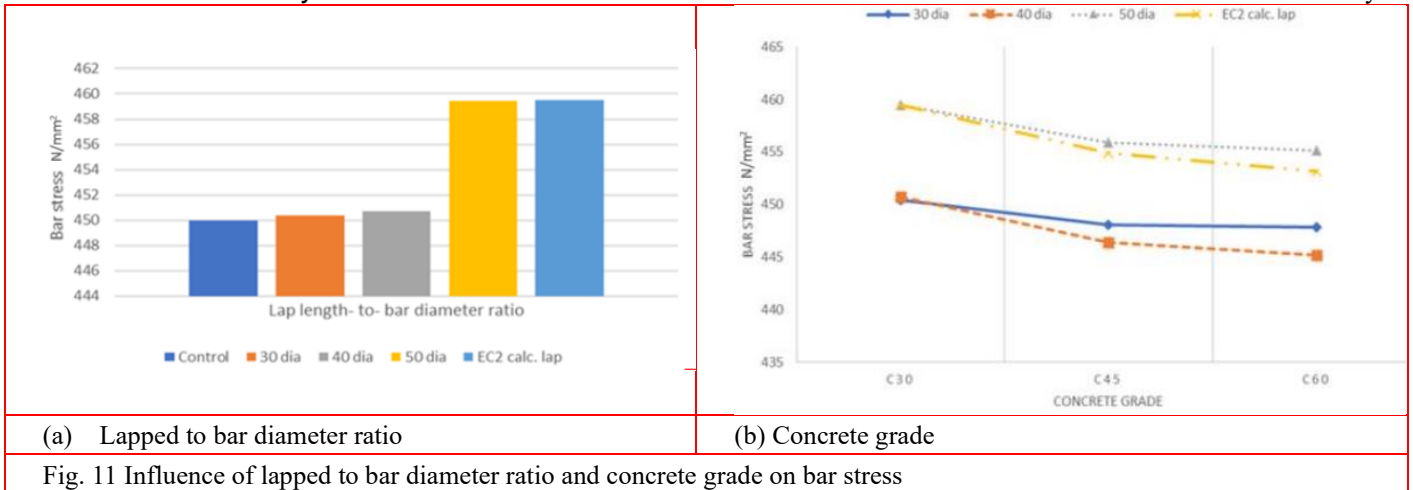
Fig. 11 Influence of lapped to bar diameter ratio and concrete grade on bar stress

The proposed finite element 2D model was employed to examine the impact of varying lap length, concrete grade, depth, and link spacing on the structural performance under ultimate load. In particular, the parameters considered are as follows • Lap length: 30∅, 40∅, 50∅ and EC2 62∅ • Shear link spacing: 100 mm and 50 mm. • Concrete grade: 30 N/mm^2, $45N/mm^2$ and $60N/mm^2$ • Zero shear distance (distance between the two-point loads) The compressive strengths were selected based on the concrete grades as provided by EN1992- 1-1:2004 (2014). The shear link spacing was chosen based on the Eurocode 2 recommended value of 0.75d. For each analysis, the value of the uniaxial tensile strength has been determined as a function of the uniaxial compressive strength employed, based on the model given by Eurocode 2 (2004): $Ec = 22(0.1fcm)^{0.3}$.

5.2. Impact of lap length on bar stress

It is generally assumed that the bar stress is constant along the splice length at failure and thus, by association, the force is uniformly distributed along the spliced bars (BS EN 1992-1-1, 2004). Figure 11(a) plots bar stress against the lap-length-to-bar diameter ratio to depict the relationship between bar stress and the lap splice length. Figure 11(a) shows that, as the lap-lengthto-bar diameter ratio increases, the bar stress increases, which corresponds well with other

distributed over the reinforcing bar length when the lap length is longer. A 107% increase in lap-length-to-bar diameter ratio leads to a 2% increase in bar stress as shown in Figure 11(a). Opposite results were found for specimens with a different concrete grade. Figure 11(b) shows the decrease in bar stress of about 0.6% for the 360 mm lap length specimens when the concrete grade increased from C30 to C60. Whereas in the case of beams with the 480 mm lap length, the reduction in bar stress was 0.2% when the concrete grade increased from C30 to C45, and a 1.2% reduction in bar stress when the concrete grade is further increased from C30 to C60. This is because the bar stress distribution along the lap length is influenced by concrete strength, partly due the slip of reinforcement and weaker concrete adjust to differential strain (CIBFIP, 1991; Lundgren, 2005).

Figure 12 shows the effect of zero shear span distance (distance between two-point loads) on the concrete grade (Figure 12[a]) and the lapped bar stress (Figure 12[b]). For the same lap-length of 360 mm, increasing the zero-shear span distance by 40% resulted in a 0.7% reduction in bar stress for beams with C30 grade of concrete, as shown in Figure 12(a). This shows that zero shear span distance is

Yakubu M. Karkarna, Ali Bahadori-Jahromi, Hamid Zolghadr Jahromi
and Emily Halliwell

inversely proportional to concrete grade. A similar trend was observed when the beams with 500 mm zero shear span distance (360 mm, 480 mm, 600 mm and 744 mm) were compared with that of 700 mm zero shear span as shown in Figure 12(b). However, the trend changed after the zero-shear span distance was increased to 900 mm as shown in Figure 12(b). This shows that the larger the zero-shear span distance the lower the lapped bar stress. The bond stress of lap splices decreases with increasing zero shear distance, irrespective of concrete grade and lap length.

5.4. Bar forces versus strain

A nonlinear relationship exists between the strain and the lap length-to-bar diameter ratio, as shown in Figure (14a). This indicates that for every increase in lap length-to-bar diameter ratio, there is a similar increase in the obtained strain for the RC beam. It can also be suggested that the lap length to-bar diameter ratio influences the overall strain of a RC beam. This is evidenced by the data trend shown in Figure 14(a). Increasing the lap length-to-bar diameter ratio
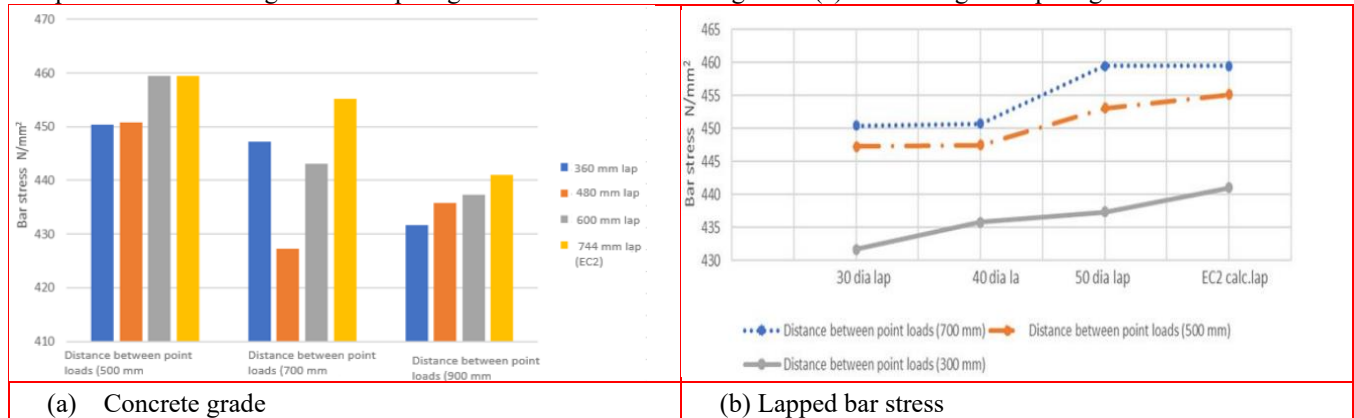
(a) Concrete grade	(b) Lapped bar stress

Fig. 12 Effect of zero-shear span distance on concrete grade and lapped bar stress

5.3. Influence of shear links spacing.

Beams with smaller shear link spacing showed greater lapped bar stress than those with larger link spacing. The bond stress and ductility of three similar specimens 30Ø, 40Ø and 50Ø, with the same cover and different shear link spacing (50 and 100 mm) were analysed in Figure 13(a) and 13(b). The shear link spacing for all the specimens are based on Eurocode 2 recommendations. It is evident that, as the shear link spacing decreases, the lapped bar stress and the load capacity of the beams increase; this behavioral response was well captured by the simulations. Figure 13(a) shows the graph of lapped bar stress against the shear link spacing. For same lap-length to bar diameter ratio of 30Ø, Increasing the shear link spacing by 100% from 50 to 100 mm resulted in a 22% increase in lap stress. The same increase was found for specimens with different concrete grades. Figure 13(b) shows 28% decrease in lapped bar stress for the 30Ø specimens when the concrete grade increased from C30 to C45.

from 30Ø to 40Ø resulted in a 215% increase in lapped bar strain. A further 25% decrease from 40Ø to 50Ø, decreased the lapped bar strain by 0.6%. The effect of concrete grade on strain in a RC beam is shown in Figure 14(b). It appears that the lapped bar strain has an inverse relationship with concrete grade as lapped bar strain decreases with an increase of concrete grade. For the same lap length-to-bar diameter ratio of 30Ø, a reduction of 29% in lapped bar stain is observed when the concrete grade is increased from C30 to C45 as demonstrated in Figure 14(b). The same pattern is noted when the concrete grade is increased from C45 to C60 Figure 14[b]. Figure 15 shows the effect of force on bar strain. Similarly, to the lapped bar stress, there is a nonlinear relationship between bar force and lap length. The maximum force in pairs of lapped bars decreases with an increase in lap length which is typical for the analysed splices and consistent with the splice being in a constant moment zone.
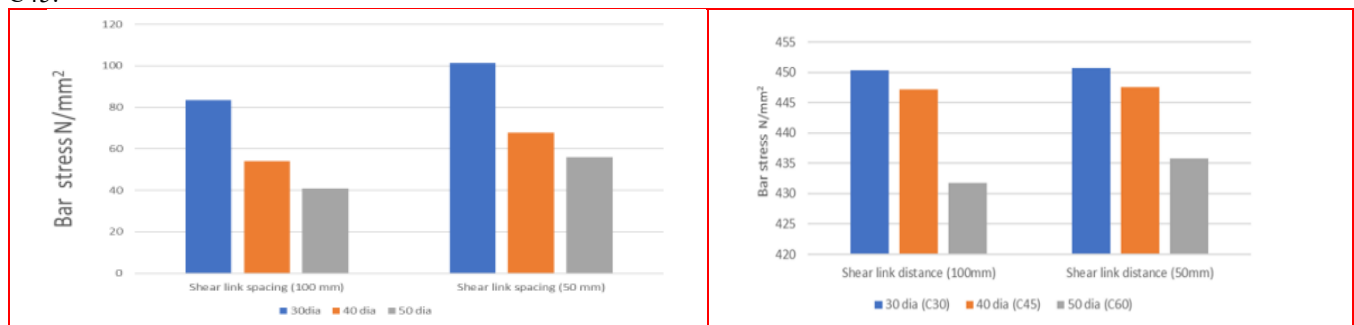
(a) Bar force	(b) Concrete grade

Fig. 13 Effect of shear link spacing on concrete grade

| (a)   Bar diameter ratio | (b) Bar force |
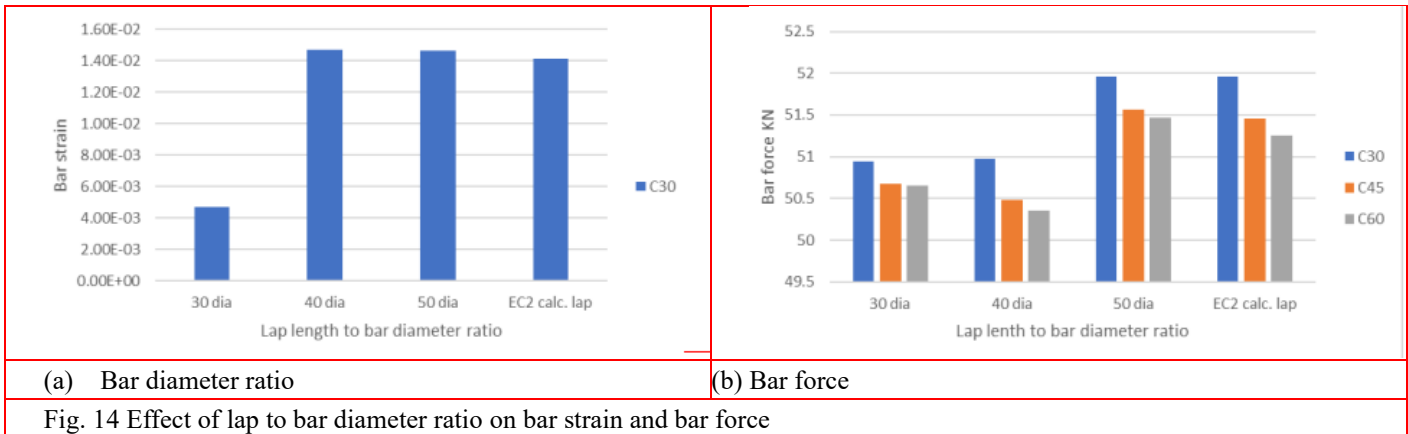
Fig. 14 Effect of lap to bar diameter ratio on bar strain and bar force
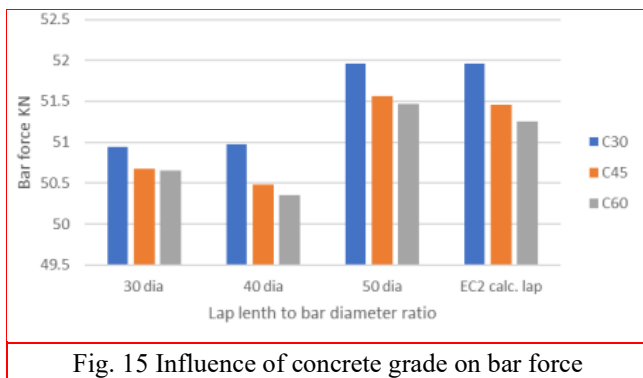

Fig. 15 Influence of concrete grade on bar force

Figure 15 shows the effect of concrete on the lapped bar force. Figure 14(a) shows the inverse relationship between the concrete grade and the lapped bar force; an increase in zero shear distance results in a decrease in the lapped bar force.

6. Conclusions

The purpose of this study was to determine the influence of concrete grade, link spacing, load location and lap length on the performance of reinforced concrete beam. This was achieved by performing experimental testing, and nonlinear finite element analyses. The finite element model was able to simulate the experimental behaviour of RC beams with and without lap splice under four-point bending. Good agreements were obtained between the experimental results and those of the finite element model in terms of ultimate load and deflection curve. Based on the behaviour model, the analysis of simulation result, the below conclusions are formed.

- Lapped bar strain and force is directly proportional to the increase in lap length-to-bar diameter ratio.
- Reduction in bar stress was noticed for all the analysed beams due to the increase in lap length-to-bar diameter ratio. Reduction in bar stress was approximately 35% when the ratio increased from 30∅ to 40∅ (33% increase).
- Reducing the shear link spacing was quite effective in delaying the formation of cracks by increasing the load carrying capacity of the samples. A comparison specimen with 50 mm and 100 mm shear link spacing indicated that smaller shear link spacing is

more effective.
- Bar stress decreases as the concrete grade is increased from C30 to C60 and the reduction for samples with lap lengths-to-bar diameter ratio of 40∅ and 50∅ were 49% and 46%, respectively.
- Zero shear span distance is inversely proportional to bond stress and bond force. Increasing the zero-shear distance by roughly 44% led to a decrease in bar stress of about 191% for beams with C30 grade of concrete.
- Increasing lap length beyond 50 diameter lap is unsustainable as well as hinders effective pouring of concrete and vibrating. As a result of the remaining air bubbles, the quality of construction and performance may be affected. It should also be noted that, while lap splicing is known as the simplest splice technique, requiring no additional skills or instruments, increasing the lapping length of the reinforcing bars can cause rebar congestion and raise construction costs.

References

ACI Committee 408, 2003. ACI 408R-03 Bond and Development of Straight Reinforcing Bars in Tension. American Concrete Institute.

Adel, A.A., Raid, A.D., and Sultan, A.D. (2020) Behavior of tension lap spliced sustainable concrete flexural members, Advanced in Concrete Construction, An International Journal, Techno-Press, Volume 9, issue 1, January 2020. https://doi.org/10.12989/ACC.2020-9.1.083 ACI Committee 408. (2003).

ACI 408R-03 Bond and Development of Straight Reinforcing Bars in Tension. In American Concrete Institute.

Anwar Hossain, K. M. (2008). Bond characteristics of plain and deformed bars in lightweight pumice concrete. Construction and Building Materials, 22(7). https://doi.org/10.1016/j.conbuildmat.2007.03.025

Akeju, T.A.I., 2018. Influence of Stirrups on Overlap Splice Strength of Epoxy Coated Deformed Bars. Construction Science, Volume 20, issue 1, pp.38–46, April 2018. https://doi.org/10.2478/cons-2017-0006

BS EN 1992-1-1. (2004). Eurocode 2: Design of concrete structures - Part 1-1 : General rules and rules for buildings. British Standards Institution, 1(2004), 230. https://doi.org/[Authority: The European Union Per Regulation

Yakubu M. Karkarna, Ali Bahadori-Jahromi, Hamid Zolghadr Jahromi
and Emily Halliwell

305/2011, Directive 98/34/EC, Directive 2004/18/EC]

Cairns, J. (2016). An evaluation of EC2 rules for design of compression lap joints. Structures, 5, 35–43. https://doi.org/10.1016/j.istruc.2015.07.004

CIBFIP. (1991). CEB-FIP model code 1990: design code. In Bulletin d'Information (Issues 213–214). Thomas Telford Services Ltd. http://books.google.com/books?hl=en&lr=&id=IRG9GTPJ7s8C&oi=fnd&pg=PR5&dq=CEBFIP+model+code+1990:+Design+Code&ots=756sbOWzgo&sig=x2_W4HCZLIqwahl62aMrKidAcTU

Do Carmo, R. N. F., & Lopes, S. M. R. (2005). Ductility and linear analysis with moment redistribution in reinforced high-strength concrete beams. Canadian Journal of Civil Engineering, 32(1), 194–203. https://doi.org/10.1139/l04-080

fib Model Code for Concrete Structures 2010. (2013). In fib Model Code for Concrete Structures 2010. wiley. https://doi.org/10.1002/9783433604090

Guizani, L., Chaallal, O., & Mousavi, S. S. (2017). Local bond stress-slip model for reinforced concrete joints and anchorages with moderate confinement. Canadian Journal of Civil Engineering, 44(3), 201–211. https://doi.org/10.1139/cjce-2015-0333

Kim, C. G., Park, H. G., & Eom, T. S. (2019). Effects of type of bar lap splice on reinforced concrete columns subjected to cyclic loading. ACI Structural Journal, 116(2), 183–194. https://doi.org/10.14359/51711142

Kim, D. J., Kim, M. S., Yun, G. Y., & Lee, Y. H. (2013). Bond strength of steel deformed rebars embedded in artificial lightweight aggregate concrete. Journal of Adhesion Science and Technology, 27(5–6). https://doi.org/10.1080/01694243.2012.687552

Karkarna, Y.M., Bahadori-Jahromi, A., Jahromi, H., Bonner, E. and Goodchild, C.(2020) Comparative study of factors influencing tension lap splices in reinforced concrete beams. Advances in Concrete Construction, An International Journal, Techno-Press

Lagier, F., Massicotte, B., & Charron, J. P. (2015). Bond strength of tension lap splice specimens in UHPFRC. Construction and Building Materials, 93. https://doi.org/10.1016/j.conbuildmat.2015.05.009

Lundgren, K. (2005). Bond between ribbed bars and concrete. Part 1: Modified model. Magazine of Concrete Research, 57(7), 371–382. https://doi.org/10.1680/macr.2005.57.7.371

Lusas. (2015). Examples Manual. In Examples Manual. Micallef, M., & Vollum, R. (2017). The Effect of Shear and Lap Arrangement on Reinforcement Lap Strength. Structures, 12, 253–264. https://doi.org/10.1016/j.istruc.2017.09.004

Mounir, A., 2018. Behavior of RC beams with tension lap splices confined with transverse reinforcement using different types of concrete under pure bending. Alexandria Engineering Journal, Volume 57, issue 3, pp.1727–1740, September 2018. https://doi.org/10.1016/j.aej.2017.05.001.

Micallef, M. (Imperial C.L. and Vollum, R.L. (Imperia. C.L., 2018. The behaviour of long tension reinforcement laps Author. Institution of Civil Engineers, Volume 70, issue 14, pp.739–755, July 2018. https://doi.org/10.1680/jmacr.17.00285

Micallef, M. and Vollum, R., 2017. The Effect of Shear and Lap Arrangement on Reinforcement Lap Strength. Structures, Volume 12, pp.253–264, November 2017. https://doi.org/10.1016/j.istruc.2017.09.004

Tovi, S., Goodchild, C. and Bahadori-Jahromi, A. (2017) Deformation of multi-storey flat slabs, a site investigation, Advances in concrete construction, An International Journal, Techno-Press, Volume 5, Issue 1, pp. 49-63, February 2017. https://doi.org/10.12989/ACC..5.1.49

Fib TG4.5, F., 2014. Bond and anchorage of embedded reinforcement: Background to the fib Model Code for Concrete Structures 2010

Wu C. H., Chen, W. Y. and Chen, H. J. (2018), "Bond Behavior of Tension Bar at Lap Splice of SCC Beam", Key Engineering Materials, pp.126-130, November 2018. https://doi.org/10.4028/www.scientific.net/KEM.789.126.

Yang, W., Yu, J., & Wang, Y. (2012). Study on the effect of bond-anchoring factor on bond behavior between deformed bar and shale ceramic concrete. Advanced Materials Research, 403–408. https://doi.org/10.4028/www.scientific.net/AMR.403-408.444

Yuan, J., O'Reilly, M., Matamoros, A., & Darwin, D. (2016). Effect of preexisting cracks on lap splice strength of reinforcing bars. ACI Structural Journal, 113(4), 801–812. https://doi.org/10.14359/51688753